Materials Science and Engineering A 396 (2005) 99–106

www.elsevier.com/locate/msea

Effect of tungsten additions on the mechanical properties of Ti-6Al-4V

Heeman Choe [a], Susan M. Abkowitz [b], Stanley Abkowitz [b], David C. Dunand [a,*]

[a] *Department of Materials Science and Engineering, Northwestern University, Cook Hall, 2220 Campus Drive, Evanston, IL 60208-3108, USA*

[b] *Dynamet Technology Inc., Eight A Street, Burlington, MA 01803, USA*

Received 1 October 2004; accepted 5 January 2005

Abstract

The alloy Ti-6Al-4V was modified by addition of 10 wt.% tungsten through powder metallurgy. Depending on the initial W powder size, different materials were formed after powder densification: (i) "alloys" for fine (0.7 and 2 μm) W powders which were almost completely dissolved in the Ti-6Al-4V matrix; (ii) "alloyed composites" for intermediate (12 and <45 μm) W powders which were partially dissolved; (iii) and "composites" for coarse (<250 μm) W powders which were nearly un-dissolved. In all cases, tungsten strengthens Ti-6Al-4V, but much more so when dissolved in the matrix than as a second phase. Ductility was not affected by W additions for the fully-dissolved alloys, but was reduced in the case of composites with W particles, which exhibited fracture or pull-out from the matrix. Flaw sensitivity was apparent from strain hardening being much lower in tension than in compression, and from a much reduced ductility exhibited by one specimen with residual porosity.

Keywords: Metal matrix composites; Titanium; Powder-metallurgy; Mechanical properties; Tungsten

1. Introduction

Titanium and titanium-based alloys are displacing stainless steel and cobalt alloys in the field of bone-replacement implant because of their excellent corrosion resistance and bio-compatibility, reduced density and lack of magnetism (of importance for magnetic resonance imaging after implantation) [1–3]. However, the hardness and wear resistance of commercial purity titanium (CP-Ti) are unsuitable for these applications [4,5], and even the harder and stronger biocompatible titanium alloys (e.g., Ti-6Al-4V or Ti-6Al-7Nb) fall far short of steel and cobalt alloys in terms of wear resistance. Recently, we have shown that adding fine tungsten powders to CP-Ti and Ti-6Al-4V produced by powder-metallurgy very significantly increased both strength and hardness (which generally scales with wear resistance), and exacted only a minor ductility penalty [6]. Furthermore, of importance for biomedical applications, tungsten has low toxicity, is non-magnetic and decreases the elastic modulus of titanium when in solid–solution [6], which helps alleviate stress-shielding arising from differences in compliance between the implant and the host tissue [5].

In a follow-up study [7], we examined the effect of W powder size upon the microstructure and mechanical properties of powder-metallurgy Ti-10 wt.% W. It was found that finer W particles dissolved almost completely during processing, resulting in a Ti-W alloys with excellent strength and ductility. By contrast, coarser W particles remained mostly un-dissolved, resulting in a composite consisting of a Ti matrix containing W particulates, with reduced strength and ductility as compared to the fully-dissolved Ti-W alloy.

In the present article, we extend the above study of W powder size (which controls the level of W dissolution) to the Ti-6Al-4V alloy, and discuss our results in terms of the relative importance of solid–solution strengthening and composite strengthening for W in Ti-6Al-4V.

* Corresponding author. Tel.: +1 847 4915370; fax: +1 847 4676573.
E-mail address: dunand@northwestern.edu (D.C. Dunand).

0921-5093/$ – see front matter © 2005 Elsevier B.V. All rights reserved.
doi:10.1016/j.msea.2005.01.051

Table 1
Initial tungsten powder and particle parameters after densification

Alloy	W powder type	Average size of initial W powders (μm)	Size of W particles in matrix[b] (μm)	Volume fraction of W particles in matrix (%)	Extent of W powder dissolution in matrix (%)	Average W concentration in matrix[c] (wt.%)
1	FSSS[a] 0.72	0.7	29 ± 12	0.02	99	9.92
2	FSSS[a] 2.02	2	25 ± 12	0.09	96	9.65
3	FSSS[a] 12.5	12	31 ± 24	0.51	80	8.13
4	−325 mesh	<45	21 ± 10	0.83	67	6.89
5	−60 mesh	<250	100 ± 71	2.47	0.6	0.06

[a] Fisher sub-sieve size.
[b] Apparent size in metallographic sections with error given as standard deviation.
[c] Calculated from measured W particle volume fraction assuming an overall W content of 10 wt.%.

2. Experimental procedures

Ti-6Al-4V/10W (all compositions are given in wt. pct) powder blends were prepared using Ti (<150 μm) powders, Al-40V master alloy powders and W powders. Five W powders were used, with size spanning over two orders of magnitude: 0.72 μm (labeled Alloy 1), 2 μm (Alloy 2), 12 μm (Alloy 3), <45 μm (Alloy 4) and <250 μm (Alloy 5), as summarized in Table 1. The powder blends were densified by the combined cold- and hot-isostatic pressing method (CHIP method [8]), as described in the following. First, green billets were produced by cold-isostatic pressing at a pressure of 379 MPa. These billets were then vacuumed-sintered at 1230 °C for 4 h and densified by hot-isostatic pressing (HIP) at 900 °C for 2 h at 100 MPa, followed by slow cooling within the press (in about 3 h). A control, W-free Ti-6Al-4V billet was produced by the same route.

The microstructure of the densified materials was examined by optical microscopy on cross-sections produced by grinding on SiC paper, polishing with diamond and alumina slurries, and etching with a modified Kroll's reagent (5% nitric acid, 10% HF, and 85% water). The volume fraction of tungsten particles was determined by automated image analysis (for Alloys 3–5) or by counting all particles present in the cross-sections and measuring optically their area (for Alloys 1–2 with very few particles present). An average value of tungsten particle size was measured on randomly-selected particles. Chemical composition profiles were measured by energy-dispersive spectroscopy (EDS, Hitachi S-3500) with a spot size of 15 nm. Matrix micro-hardness was measured with a Vickers indenter using a 200 g load and an indent time of 10 s on epoxy-mounted specimens, which had been ground and polished.

The Young's modulus was determined using an ultrasonic wave reflection technique on parallel-faced cylindrical specimens with a diameter of 6 mm and a length of 10 mm. The longitudinal and transverse speeds of sound were measured using 50 MHz transducers connected to a digital oscilloscope. Molasses was employed as a coupling agent between the transducers and the specimens. The Poisson's ratio and Young's modulus of the monolithic Ti-6Al-4V and Ti-6Al-4V/10W alloys were then calculated according to Ref. [9], using the measured longitudinal and transverse speeds of sound and their density.

Tensile tests were preformed at ambient temperature on one specimen of each alloy, machined to ASTM E-8 proportional standards with 36 mm gauge length and 6.4 mm gauge diameter. The cross-head speed was 12.7 mm/min, corresponding to an initial strain rate of $6.2 \times 10^{-3}\,s^{-1}$. Strain was measured using a clip-on extensometer with 25.4 mm gauge length. Fracture surfaces were imaged in a scanning electron microscope (SEM).

Compressive tests were carried out at ambient temperature on one cylindrical specimen of each alloy, with a diameter of ∼7 mm and an aspect ratio of 3:1, according to ASTM standards E-9. The tests were carried out to engineering strains of ∼20% until fracture (which occurred by shearing), maintaining a low strain rate of $1 \times 10^{-4}\,s^{-1}$ using a computer-controlled servo-hydraulic test system. The specimens were deformed within a steel compression cage outfitted with polished carbide insert to maintain stress uniaxiality. Strain was determined from cross-head displacement, after correcting for machine elasticity.

3. Results

3.1. Microstructure

Billet density was 4.82 g/cm^3 for Alloys 1–3, exceeding slightly the rule-of-mixture density of 4.80 for Ti-6Al-4V/10W. Alloy 5 had a density of 4.85 g/cm^3, probably from a slightly higher W content than the nominal 10% value. Alloy 4 displayed a density of 4.79 g/cm^3 due either to a W content lower than nominal or to residual porosity.

Fig. 1(a–f) show micrographs of etched cross-sections for Alloys 1–5 and monolithic Ti-6Al-4V, exhibiting the following features: (i) white particles; (ii) a surrounding dark-etched shell, ∼50 μm thick; (iii) an etched acicular matrix. These features were identified previously [6] as: (i) partially dissolved W particle, generally existing as a discrete and discontinuous phase; (ii) matrix diffusion zone with high W content; (iii) matrix with Widmanstätten α/β structure with most of the W segregated in the β-phase. As displayed

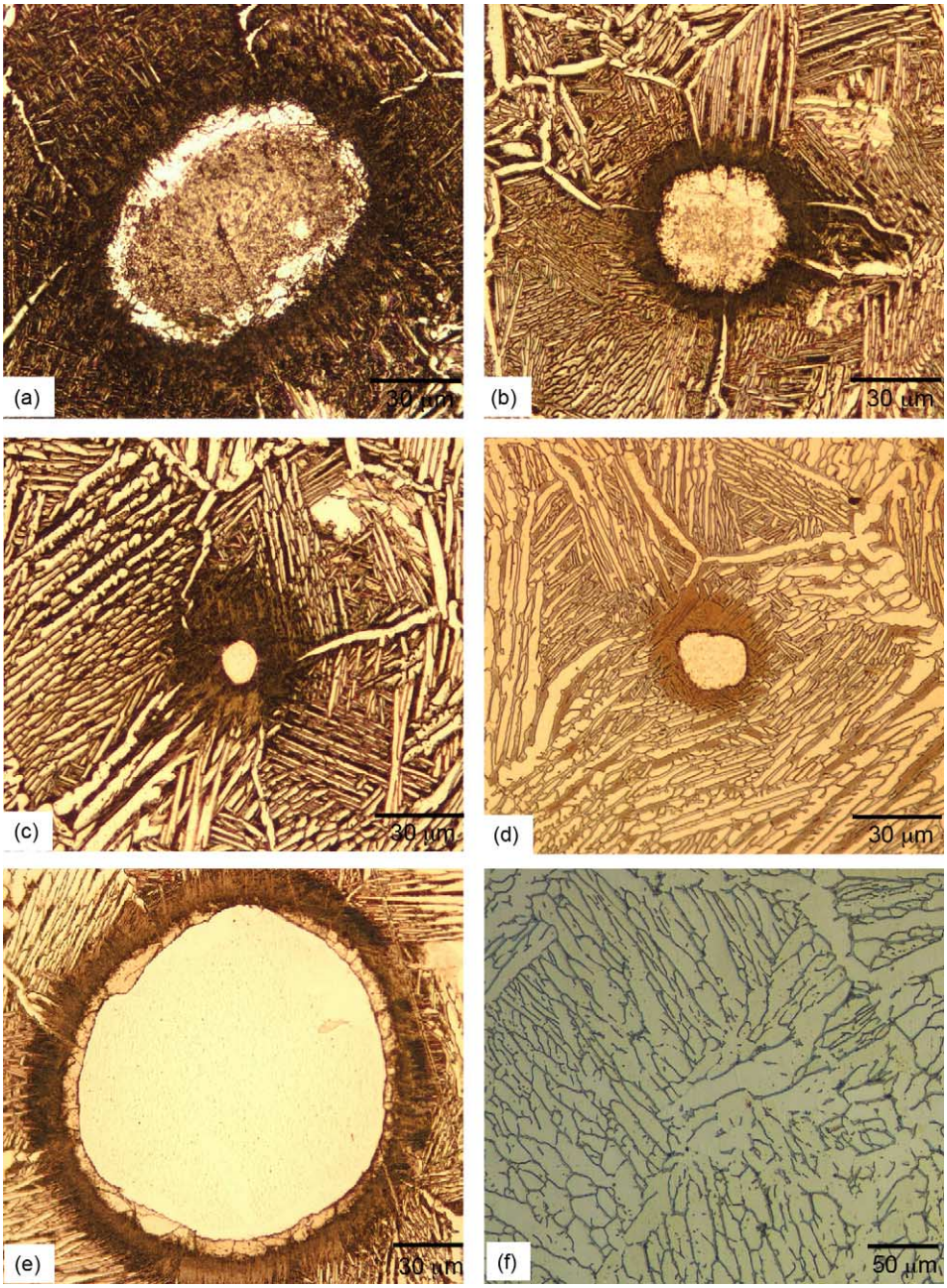

Fig. 1. Optical micrographs of densified materials, showing a W particle, an adjacent dark-etched matrix shell with high W content and the surrounding α/β etched matrix. (a) Alloy 1; (b) Alloy 2; (c) Alloy 3; (d) Alloy 4; (e) Alloy 5 and (f) monolithic Ti-6Al-4V alloy.

in Table 1, the average size of un-dissolved W particles is similar for Alloys 1–4 (about 25 μm) but much larger in Alloy 5 (about 100 μm), as expected from the much larger initial powder size for the latter alloy. While the W particle size is similar for Alloys 1–4, the volume fraction of W particles varies systematically, increasing from Alloy 1 with a very small value of 0.02 vol.% to Alloy 4, with 0.83 vol.%. Alloy 5 has much higher W particle volume fraction of 2.47 vol.%. Again, this trend is expected, as smaller W powders dissolve more completely than coarser one during processing. Table 1 summarizes the W particle size and volume fraction, as well as the calculated average matrix W content.

SEM observation at higher magnification (Fig. 2(a)) shows that, for Alloy 1 processed from fine 0.7 μm W powders, the few large W particles remaining in the matrix after processing consist of agglomerates of fine, micron-size W particulates whose interstices are filled with titanium alloy matrix; the particle/matrix interface is irregular and diffuse. By contrast, in Alloy 5 processed with large <250 μm W powders (Fig. 2(b)), the W particles are monolithic and their interface with the matrix is sharp and free of any reaction layer.

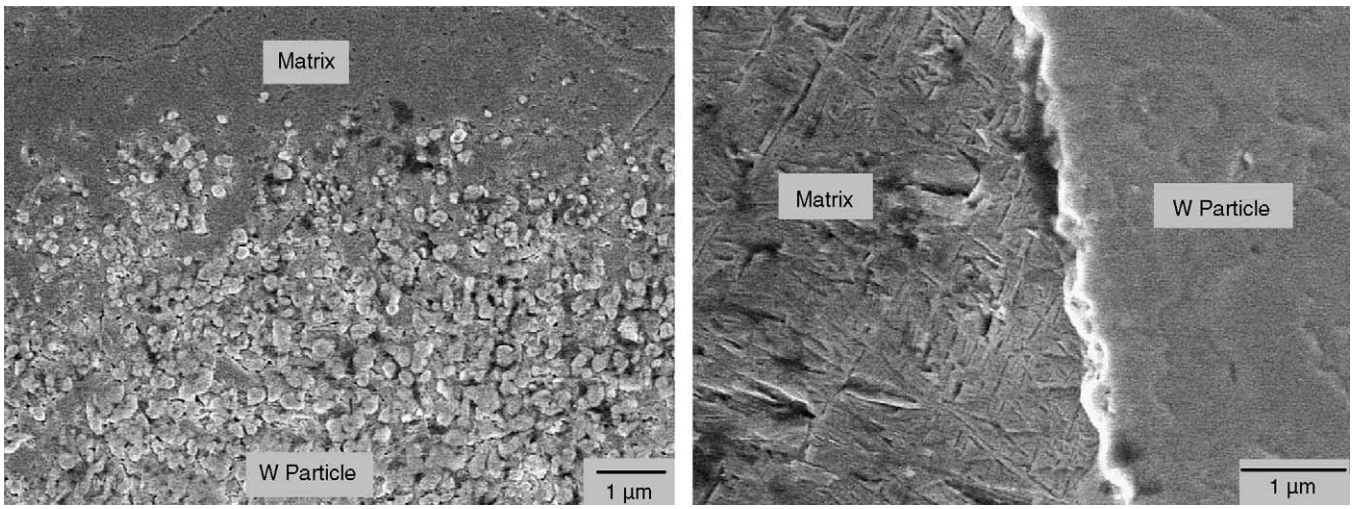

Fig. 2. SEM micrographs showing the interfacial regions of a W particle (a) Alloy 1, where the particle is an agglomerate of fine W particulates; (b) Alloy 5, where the particle is monolithic.

Fig. 3 displays EDS composition profiles for Alloys 1, 4 and 5, measured from the center of a W particle through the diffusion zone and into the matrix. For Alloy 4 and 5, the W content decreases from 100% (as expected for a monolithic particle) to the expected average matrix composition (6.9 and 0.1%, Table 1) over a distance of about 140 μm. For Alloy 1, the concentration gradient is less steep, varying from 74% at particle center (as expected for an agglomerated particle containing Ti-6Al-4V, Fig. 2(a)) to ∼10% in the matrix, over a distance of about 200 μm.

3.2. Mechanical properties

Fig. 4 shows the tensile stress–strain curves at ambient temperature for Alloys 1–5, compared with that of the W-free Ti-6Al-4V control alloy. Alloys 1 and 2, with almost all W dissolved, have nearly overlapping stress–strain curves with yield and ultimate strengths higher by about 20% as compared to those of Ti-6Al-4V. These alloys also show considerable necking, with ductility values similar to that of Ti-6Al-4V. The strength and ductility values for Alloy 3 (with 80% of its tungsten dissolved and 20% un-dissolved as particle) are lower than for Alloys 1–2, and this trend is continued with Alloy 5 (with almost all its W in the form of particles), where yield and ultimate strengths are higher by 5% but ductility is lower by 37% as compared to Ti-6Al-4V. Alloy 4 (with two thirds of its tungsten dissolved) has strengths similar to Alloy 3, but fractured prematurely after reaching its ultimate tensile strength.

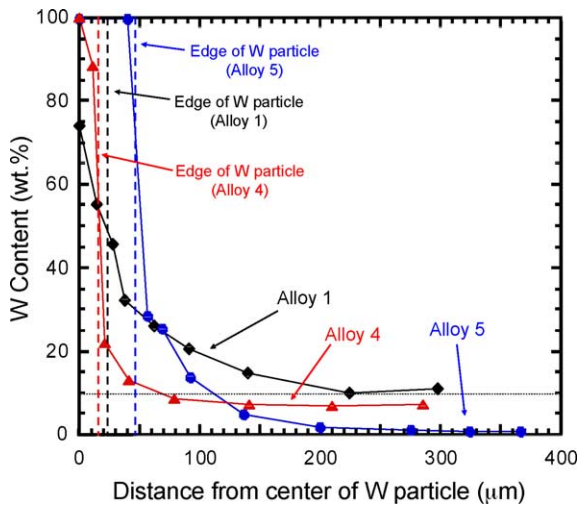

Fig. 3. EDS composition profiles from the center of an arbitrarily selected W particle into the Ti matrix for Alloys 1 and 4 (with most W dissolved) and Alloy 5 (with most W un-dissolved).

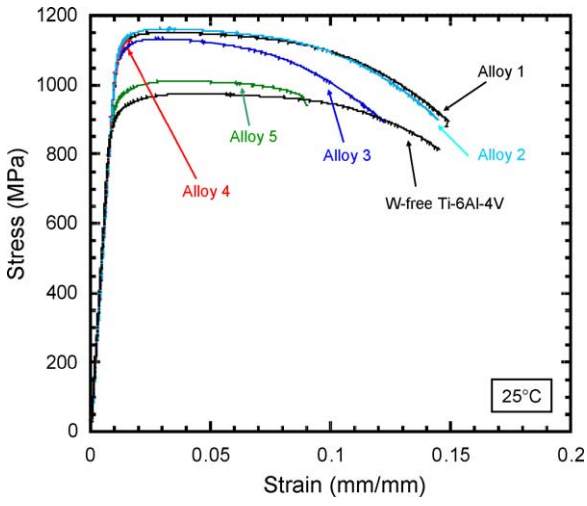

Fig. 4. Tensile stress–strain curves for Alloys 1 and 2 (with almost all W dissolved), Alloys 3 and 4 (with a majority of W dissolved) and Alloy 5 (with almost none of W dissolved). Also shown for comparison is the curve for the control W-free Ti-6Al-4V produced by the same powder-metallurgy route.

Table 3
Compressive properties

Alloy	0.2% Yield stress (MPa)	Strain at failure (%)
Ti-6Al-4V	918	>25
1	1040	18.6
2	1070	17.0
3	1070	18.0
4	1120	18.1
5	910	22.3

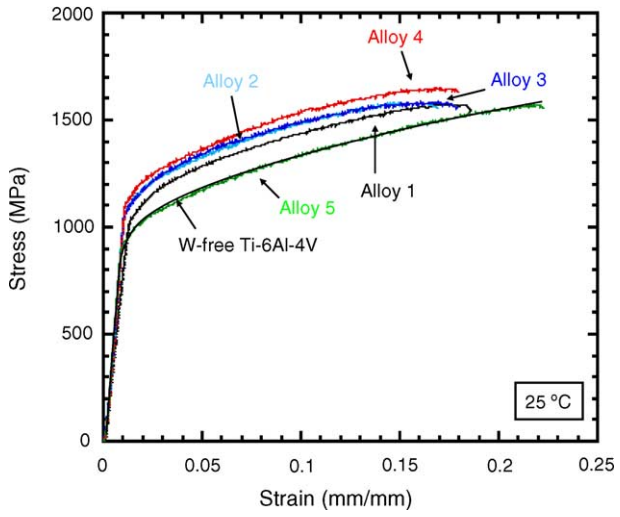

Fig. 5. Compressive stress–strain curves of Ti-6Al-4V/10W and control W-free Ti-6Al-4V.

The tensile properties are tabulated in Table 2, which also includes a Ti-6Al-4V/10W alloy produced from 3 μm W powders reported in Ref. [6], whose mechanical properties are in reasonable agreement with those of Alloy 2 (made with 2 μm W powders). Table 2 also shows the ultrasonically-measured elastic moduli: the addition of 10% W to Ti-6Al-4V affects very minimally the elastic modulus of Ti-6Al-4V, but increases by about 25% the micro-hardness of the matrix, with the exception of Alloy 5 with little W dissolved in its matrix.

The compressive stress strain curves for Alloys 1–5 are presented in Fig. 5 as compared to that of the W-free Ti-6Al-4V control alloy. The main differences with respect to the tensile curves in Fig. 4 are: lower yield stress (except for Alloy 4); much higher strain hardening rates; much higher ultimate compressive stresses, and higher fracture strain (much higher in the case of Alloy 4, which fractured at 1.6% in tension). As was observed in tensile stress–strain behavior, the addition of 10% W to Ti-6Al-4V improved the compressive yield strength by 13–22%, except for Alloy 5 with a slight decrease in yield strength from 918 to 910 MPa (Table 3).

SEM pictures of tensile fracture surfaces for Alloys 1 and 5 are shown in Fig. 6. The strongest and most ductile Alloy 1 exhibits pockets of spherical dimples in the matrix (Fig. 6(a)), typical of ductile fracture. By contrast, for the least strong and less ductile Alloy 5, matrix dimples are much larger than for Alloy 1 (Fig. 6(b)), and evidence of W particles brittle fracture (Fig. 6(c)) and pull-out (Fig. 6(d)) is observed.

4. Discussion

4.1. Microstructure

In binary Ti-W alloys, there is complete solubility between β-Ti and W above 882 °C [10]. For Ti-6Al-4V, which consists of a majority α-phase at ambient temperature under standard heat treatment conditions, the β-transus is near 990 °C [11]. Based on these two facts, it is expected that the sintering treatment at 1230 °C (and to a lesser extent the HIP treatment at 900 °C) promoted dissolution of the W particles. The W particle volume fractions listed in Table 2 indicate that there was almost complete dissolution (>95%) for Alloys 1 and 2 with the finest (0.7 and 2 μm) powders, partial dissolution (∼75%) for Alloys 3 and 4 with coarser (12 and <45 μm) powders, and almost no dissolution (<1%) for Alloy 5 with the coarsest (<250 μm) powders. A similar trend was observed previously for a series of Ti-10W alloys [7], reflecting an increasing dissolution extent with decreasing W particle diameter. The W particles present in Alloys 1 and 2 probably correspond to "stray" particles much larger than the average value (for example, the manufacturer reports that 3% of the nominally <45 μm powders exceed the −325 mesh specification).

For a similar Ti-6Al-4V/10W alloy made with fine 3 μm W powders [6], it was found that W stabilizes the β-phase in which W is partitioned to a level of 11 ± 1% (as compared to 2.5 ± 0.8% in the minority α-phase). The matrix

Table 2
Tensile properties and matrix hardness

Alloy	0.2% Yield stress (MPa)	Ultimate tensile stress (MPa)	Strain at failure (%)	Young's modulus[a] (GPa)	Matrix hardness (HV)
Ti-6Al-4V	902	975	14.5	117	332 ± 19
1	1116	1162	14.5	114	436 ± 19
2	1103	1152	14.8	112	414 ± 15
3	1072	1133	12.2	114	432 ± 16
4	1101	1130	1.6	113	426 ± 20
5	944	1012	9.1	114	376 ± 13
Ti-6Al-4V/10W [6]	1160	1280	6.8	108	406 ± 10

[a] Ultrasonic measurement.

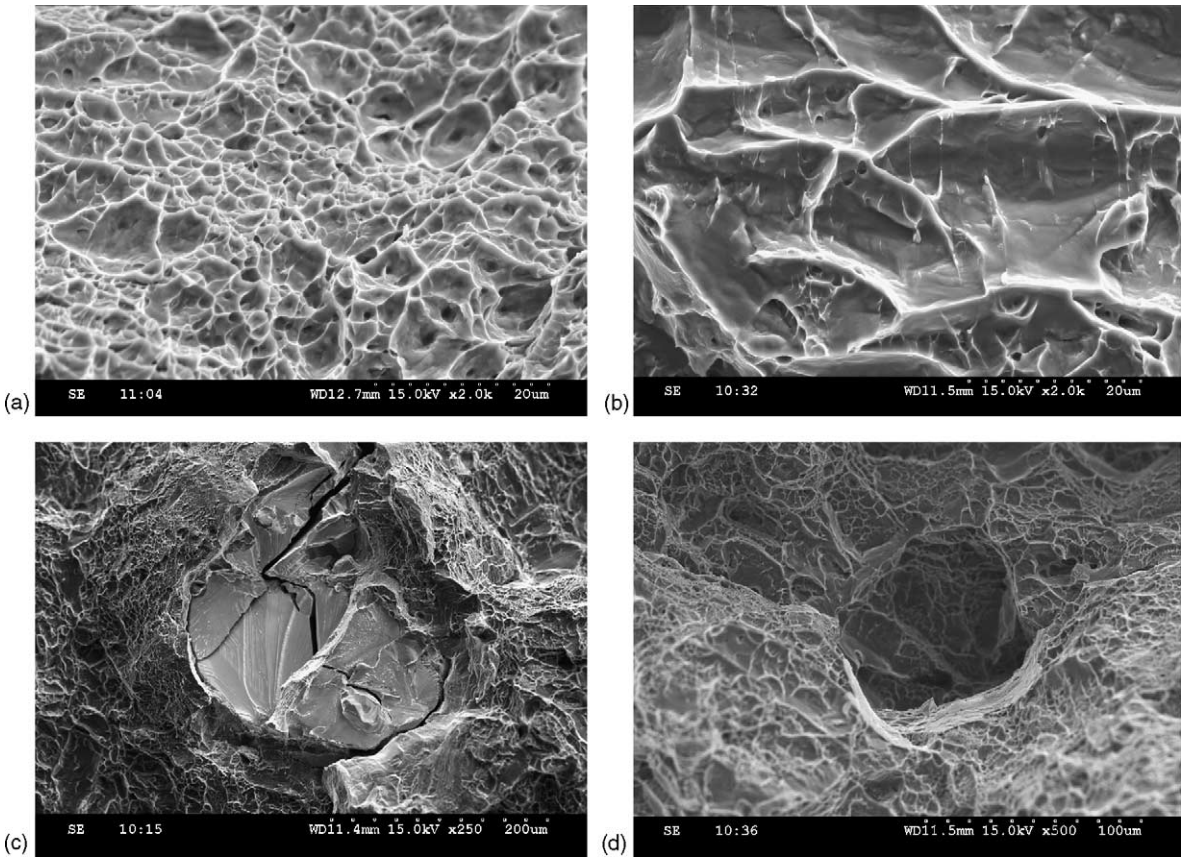

Fig. 6. SEM micrographs of tensile fracture surfaces showing (a) pockets of dimples in the matrix of Alloy 1, typical of ductile failure; (b) relatively large matrix dimples in Alloy 5; (c) brittle failure of a reinforcing W particulate by cracking in Alloy 5 and (d) a large depression due to W particle pull-out from the matrix in Alloy 5.

of the present alloys (Fig. 1(a–d)) exhibits the same two-phase, Widmanstätten α/β structure (with the β-phase as the majority phase) as that found in this previous study [6], and it can thus be expected that similar partitioning to the β-phase is present; however, its extent may vary from the above values depending on the level of W particle dissolution.

The un-dissolved tungsten particles are surrounded by a matrix diffusion zone, discernible optically after etching in Fig. 1(a–e), with higher W content (Fig. 3). Micro-hardness performed on similar diffusion zone in Ti/10W has shown that hardness is lower in the diffusion zone than in the matrix far from the particles: the hard W particles are thus surrounded by a softer matrix shell.

4.2. Mechanical properties

The Young's modulus (measured by the ultrasonic method) was affected only little by the presence of tungsten, with a drop of about 4 GPa for all alloys, from a value of 117 GPa for Ti-6Al-4V. A relatively larger decrease of about 8 GPa was reported previously for Ti-6Al-4V/10W produced from fine powders [6]. This discrepancy may be due to the slower cooling rate (by about a factor 5) used following HIP consolidation for the present alloys, which may have affected the formation of various metastable phases known to exist in Ti-W alloys [11–13].

Two strengthening mechanisms can be identified for the increase in strength and hardness of the Ti-6Al-4V/10W alloys as compared to monolithic Ti-6Al-4V alloy. The first is solid–solution strengthening by W solute atoms of either stabilized or martensitically-transformed β-phase, which is influenced by the W content of the matrix, both average and local (precipitation strengthening might also occur if W-rich precipitates form on cooling from the processing temperature, but is not considered here). The second mechanism is composite strengthening by W particles, which is affected by their volume fraction, size and shape. The load transfer effect on yield strength is, however, expected to be insignificant (less than 10 MPa [7]), given the low volume fraction and equiaxed shape of the W particles. Moreover, indirect composite strengthening by thermal-mismatch dislocations and grain size refinement is similarly negligible given the low volume fraction and relatively large size of the W particles. Finally, W particles are much too large for any effective dispersion strengthening. We thus conclude that composite strengthening is insignificant as compared to solid–solution strengthening.

Micro-hardness provides a local measurement of matrix strengthening due to W additions. Table 2 shows that the matrices of Alloys 1–4 exhibit the same hardness, within experimental error (ca. 425 HV). These values exceed those for pure annealed W (350–360 HV [14,15]) and Ti-6Al-4V (332 HV, Table 2), illustrating the strong hardening effect of W in solution within the matrix, which is also expected to increase the wear resistance of these alloys. There is however no difference with previously reported values of hardness in fully-dissolved Ti/10W (ca. 430 HV), indicating that the hardening effect of Al and V is masked by the very strong effect of W. By contrast, the lower W content in the matrix of Alloy 5 leads to a lower hardness of 376 HV. This is still substantially higher than the control specimen Ti-6Al-4V (332 HV), indicating that small quantities of W (0.06% on average for the matrix of Alloy 5, but higher values near the particles, Fig. 3) are very potent in their hardening effect, while much larger quantities (7–10% for Alloys 1–4) bring only a relatively modest further improvement in hardness. This may be due to the formation of softer, non-equilibrium phases, as noted previously for Ti/10W alloys [7].

As for hardness, the yield and ultimate tensile strengths of Alloys 1–4 are virtually identical, indicating that increasing the matrix average W composition from ca. 7% (Alloy 4) to ca. 10% (Alloy 1) is not accompanied by any gain in strength. By contrast Alloy 5 shows lower strengths, which are however higher than for W-free Ti-6Al-4V. For this alloy, yielding is controlled by the W-poor matrix regions between the W particles and their associated W-rich matrix regions. The volume fraction of W-poor regions is estimated as 60%, determined by considering a W content of 1.9 wt.% at a distance of 200 μm from the particle center (Fig. 3) and an average particle diameter of 100 μm (Table 1).

The yield strength values are similar in tension and compression (within an error band of ±15 MPa) for Alloys 2–5 (the reason for the low compressive stress for Alloy 1 is unclear). A striking difference between the tension and compression curves is the much higher strain hardening rate in compression, with stresses in excess of 1500 MPa reached for all alloys after ca. 20% deformation in compression, as compared to ultimate tensile strength of ca. 1150 MPa. One likely reason for the low strain hardening in tension is the accumulation of damage in the form of cavitation, thus reducing the effective cross-section of the alloy and inducing stress concentrations. Another possibility for the W-free Ti-6Al-4V alloy is an intrinsic tension–compression asymmetry due to different deformation mechanisms, i.e., slip and twinning. This does not apply to Alloys 1–4 which exhibit little α-phase.

It is notable that the increased strength for the nearly fully homogenous Alloys 1–2 with respect to Ti-6Al-4V is not accompanied by a loss in ductility. Alloy 3 with about 0.5 vol.% W particles is somewhat less ductile and this trend is continued with Alloy 5 with 2.5 vol.% W particles, which nevertheless displays a useful ductility of 9.1%. For the high-ductility Alloys 1–2, it is apparent that the inherent ductility of the Ti-6Al-4V/10W matrix (as illustrated by the fine dimples typical of ductile tensile fracture, Fig. 6(a)) controls the overall fracture behavior, in spite of the occasional presence of W particles (Table 1). The lower ductility of Alloy 5 is then not due to the limited ductility of its matrix but to the presence of the large, brittle W particles. Indeed, Alloy 5 shows evidence of brittle failure of W particles, as shown in Fig. 6(c), indicative of strong interfacial matrix/particle bonding. Also, a small fraction of particles seem to have been pulled-out from the matrix, in particular, for relatively small W particles (<80 μm), indicative of reinforcement/matrix failure (Fig. 6(d)). Both of these incidences are known in metal matrix composites to lead to a relatively brittle fracture behavior [16–18]. A tendency in forming clustered particles can also be the governing mode of fracture [19,20] as discussed in a previous study on Ti-10W alloys [7], though this fracture mode is unlikely in Alloy 5, because particle clustering was rare.

Finally, Alloy 4 shows an unusually low ductility in tension (1.6%), but is very ductile in compression (>20%, similar to the other alloys). Together with the lower density of Alloy 4 as compared to the other alloys, these results are indicative of residual porosity (<1%, based on density) and a high sensitivity to internal flaws. This hypothesis is also corroborated by the large difference in strain hardening in tension versus compression.

5. Conclusions

- Ti-6Al-4V/10W materials were produced by powder metallurgy using fine (0.7–2 μm), intermediate (12 to <45μm) and coarse (<250 μm) W powders. After consolidation, almost all the W is dissolved within the Ti matrix for the materials with the finest W powders, which are thus solid–solution "alloys" with a transformed α/β microstructure at ambient temperature. By contrast, for the materials with the coarsest W powders, most of the W remains undissolved in the form of large metallic particles, resulting in a particulate-reinforced "composite". Materials with intermediate W powders exhibit W both in solid–solution and as particles, and are thus "alloyed composites".
- The strength of the Ti-6Al-4V/10W alloys and alloyed composites is much higher than that of the composite, indicating that W is more efficient as a solid–solution strengthener than as a particle strengthener.
- The hardness of the Ti-6Al-4V/10W alloys and alloyed composites is higher than that of the composite; values of ∼425 HV were achieved indicative of enhanced wear resistance.
- The Ti-6Al-4V/10W alloys are also more ductile than the composite, which suffers from particle pull-out and fracture. One of the Ti-6Al-4V/10W alloyed composites was brittle in tension, probably as a result of residual porosity.
- For all materials, compressive deformation leads to high strain hardening rate and ultimate compressive stresses

in excess of 1500 MPa. By contrast, tensile deformation shows little strain hardening, most likely due to cavitation.

Acknowledgement

This research was supported by NIH through a SBIR grant to Dynamet Technology Inc. (grant no. 2R44EB001005-02).

References

[1] H. Guleryuz, H. Cimenoglu, Biomaterials 25 (2004) 3325–3333.
[2] Y. Okazaki, E. Gotoh, Mater. Trans. 43 (2002) 2943–2948.
[3] M. Aziz-Kerrzo, K.G. Conroy, A.M. Fenelon, S.T. Farrell, C.B. Breslin, Biomaterials 22 (2001) 1531–1539.
[4] D. Iijima, T. Yoneyama, H. Doi, H. Hamanaka, N. Kurosaki, Biomaterials 24 (2003) 1519–1524.
[5] J. Black, Biological Performance of Materials: Fundamentals of Biocompatibility, third ed., Marcel Dekker, Inc., New York, 1999.
[6] M. Frary, S. Abkowitz, S.M. Abkowitz, D.C. Dunand, Mater. Sci. Eng. A344 (2003) 103–112.
[7] H. Choe, S. Abkowitz, S.M. Abkowitz, D.C. Dunand, J. Alloys Compd., in press.
[8] S. Abkowitz, P.F. Weihrauch, S.M. Abkowitz, Ind. Heat 12 (1993) 32–37.
[9] E. Schreiber, O.L. Anderson, N. Soga, Elastic Constants and Their Measurement, McGraw-Hill, New York, 1973.
[10] J. Murray (Ed.), Phase Diagrams of Binary Titanium Alloys, American Society for Metals, Metals Park, 1987.
[11] R. Boyer, G. Welsch, E.W. Collings (Eds.), Materials Properties Handbook: Titanium Alloys, American Society for Metals, Metals Park, 1994.
[12] E.W. Collings, The Physical Metallurgy of Titanium Alloys, American Society for Metals, Metals Park, 1984.
[13] J.C. Williams, B.S. Hickman, Metall. Trans. 1 (1970) 2648–2650.
[14] C.J. Smithells (Ed.), Smithells Metals Reference Book, seventh ed., Butterworth-Heinemann, Boston, 1992.
[15] P.B. Bardes (Ed.), Metals Handbook, vol. 2, ninth ed., American Society for Metals, Metals Park, 1979.
[16] S. Seshan, M. Jayamathy, S.V. Kailas, T.S. Srivatsan, Mater. Sci. Eng. A363 (2003) 345–351.
[17] T.S. Srivatsan, M. Al-Hajri, C. Smith, M. Petraroli, Mater. Sci. Eng. A346 (2003) 91–100.
[18] Y.L. Shen, J.J. Williams, G. Piotrowski, N. Chawla, Y.L. Guo, Acta Mater. 49 (2001) 3219–3229.
[19] J. Segurado, C. González, J. LLorca, Acta Mater. 51 (2003) 2355–2369.
[20] S.J. Hong, H.M. Kim, D. Huh, C. Suryanarayana, B.S. Chun, Mater. Sci. Eng. A347 (2003) 198–204.